Dosimetric properties of an amorphous silicon electronic portal imaging device for verification of dynamic intensity modulated radiation therapy

Peter B. Greer[a] and Carmen C. Popescu
Department of Medical Physics, B.C. Cancer Agency, Vancouver Island Centre, 2410 Lee Avenue, Victoria V8R 6V5, Canada

(Received 2 July 2002; accepted for publication 21 April 2003; published 20 June 2003)

Dosimetric properties of an amorphous silicon electronic portal imaging device (EPID) for verification of dynamic intensity modulated radiation therapy (IMRT) delivery were investigated. The EPID was utilized with continuous frame-averaging during the beam delivery. Properties studied included effect of buildup, dose linearity, field size response, sampling of rapid multileaf collimator (MLC) leaf speeds, response to dose-rate fluctuations, memory effect, and reproducibility. The dependence of response on EPID calibration and a dead time in image frame acquisition occurring every 64 frames were measured. EPID measurements were also compared to ion chamber and film for open and wedged static fields and IMRT fields. The EPID was linear with dose and dose rate, and response to MLC leaf speeds up to 2.5 $cm\,s^{-1}$ was found to be linear. A field size dependent response of up to 5% relative to d_{max} ion-chamber measurement was found. Reproducibility was within 0.8% (1 standard deviation) for an IMRT delivery recorded at intervals over a period of one month. The dead time in frame acquisition resulted in errors in the EPID that increased with leaf speed and were over 20% for a 1 cm leaf gap moving at 1.0 $cm\,s^{-1}$. The EPID measurements were also found to depend on the input beam profile utilized for EPID flood-field calibration. The EPID shows promise as a device for verification of IMRT, the major limitation currently being due to dead-time in frame acquisition.
[DOI: 10.1118/1.1582469]

Key words: EPID, electronic portal imaging device, verification, intensity modulated radiation therapy, portal dosimetry

I. INTRODUCTION

Due to its complexity, dynamic intensity modulated radiation therapy (IMRT) presents a challenge to verify that the desired fluence and hence dose distribution is delivered by the linear accelerator. One approach to IMRT verification is to transfer the IMRT fluences for each field to a test phantom and calculate the cumulative dose distribution with the radiotherapy treatment planning system (RTPS). These fields can then be delivered to the test phantom setup on the linear accelerator, the dose distribution measured (generally with film), and the result compared to the RTPS dose calculation.[1] This procedure is, however, time-consuming involving recalculation of the IMRT plan, set-up time on the linear accelerator, film processing and digitization, and comparison to the plan. Frequent film calibration and processor quality assurance is also necessary.

An alternative approach to ensure the integrity of the IMRT delivery is to verify the fluence or dose delivered for each field. In this case the fluence can be transferred to a flat phantom and the dose at a plane in the phantom calculated by the RTPS. A measurement of the delivered dose for the field made with film can be compared to an expected dose calculated by the RTPS system.[2,3] The accuracy of the RTPS dose calculation algorithm to calculate dose based on a given input fluence and patient anatomy would be verified separately as part of the commissioning process for IMRT.[4] However this approach again requires a large workload.

Electronic portal imaging devices (EPIDs) present an attractive possibility to verify IMRT delivery due to their two-dimensional digital format. Multiple verification images can also be rapidly acquired without the necessity to re-enter the treatment room to position film. For pre-treatment verification the EPID image can be compared to a predicted portal dose image (PDI) calculated from the fluence map for the field.[5,6] Another potential application is to verify the dose delivery *in vivo* with the EPID image acquired during the IMRT treatment, by comparison to a predicted transmission image.[7,8]

Until recently video-camera and liquid-ion chamber based EPIDs have been utilized for these applications. The dosimetric properties of these types of EPIDs have been extensively studied.[9–11] More recently their application to verification of dynamic IMRT has been addressed.[5,6] However, flat-panel amorphous silicon based EPIDs are rapidly replacing these EPIDs due to their superior image quality for treatment setup verification.[12] El-Mohri *et al.*[13] studied the dosimetric properties of their in-house developed amorphous silicon imager, while McCurdy *et al.*[14] investigated some basic properties for static field dosimetry. The dosimetric properties of amorphous silicon EPIDs and their applicability for

dynamic IMRT verification are therefore of current interest.

In this study the dosimetric properties of an amorphous silicon EPID for verification of dynamic IMRT were investigated. These properties included effect of buildup, dose response, field size response, relative dosimetry accuracy, response to rapid MLC leaf speeds, and beam dose-rate fluctuations. The dependence of response on EPID calibration and a dead time in image frame acquisition occurring every 64 frames were measured, as was the reproducibility for absolute dosimetry. The EPID was also compared to ion chamber and film measurements for IMRT test patterns.

II. METHODS AND MATERIALS

A. EPID and image acquisition

The amorphous silicon EPID (aS500, Varian, Palo Alto, CA) consists of a 1 mm copper metal plate, a 134 mg/cm^2 gadolinium oxysulphide phosphor screen (Kodak, Lanex Fast B) that includes a 0.18 mm polyester reflector, and a 40×30 cm^2 (512×384 pixel) a-Si array. Each pixel consists of a light sensitive photodiode and a thin-film transistor with a pixel pitch of 0.78×0.78 mm^2. The copper plate lies beneath a 10-mm-thick foam layer with 1 mm of epoxy for binding. The scintillator and amorphous silicon array ($\sim$1 mm thick) are bound to the underside of the copper plate and are enclosed between thin layers of black paper to prevent light scatter from the copper plate or components beneath the array, reaching the array. Beneath this lies a further 8 mm of foam and 1 mm epoxy. A 1.6-mm-thick plastic collision cover (epoxy with glass and foam) encloses the detector with an air gap of approximately 1.5 cm between the cover and the detector surface. The EPID was integrated with a 6EX (6 MV) linear accelerator with a dynamic multileaf collimator (DMLC) with 1 cm leaf width from the same manufacturer. All investigations were performed with a nominal beam dose rate of 400 MU min^{-1} (6.7 MU s^{-1}).

Image acquisition is controlled by the Acquisition CPU (IAS2) located in the treatment room. An image frame is scanned row by row, with a fixed number of rows scanned per beam pulse. Each individual image frame is acquired in $\sim$0.125 s at a 400 MU/min dose rate. This frame time varies slightly depending on the nominal dose-rate setting of the accelerator. To record an IMRT delivery with this EPID system, there are two possible modes of operation, multiple image acquisition and continuous frame averaging. In the first mode, multiple images are acquired during radiation delivery, with each image being the average of a fixed number of frames. In this case, however there is a delay between each acquired image due to the transfer of the image from the Acquisition CPU to the disk and database. This delay is not fixed and can be more than 2 s.[15] This mode is unlikely to be used to verify dynamic IMRT where leaf speeds of up to 3 cm s^{-1} are possible.[16] In the continuous frame-averaging mode that was used in this work, a single image consisting of the average of many image frames is acquired during radiation delivery. The EPID will average successively acquired frames up to a limit of 9999 frames.

The EPID image $I(x,y)$ obtained from continuous frame averaging is therefore:

$$I(x,y)=\frac{1}{N}\sum_{j=1}^{N} I_j(x,y), \tag{1}$$

where $I_j(x,y)$ is the jth image frame, and N is the total number of frames acquired.

B. EPID calibration

The EPID is calibrated by the acquisition of dark-field (DF) and flood-field (FF) images. The DF image is acquired with no radiation and records the pixel offsets. The FF image is recorded with an open field ''uniform'' irradiation to determine differences in individual pixel sensitivities. When an image is acquired by the EPID the DF is subtracted and the image is then divided by the normalized FF image:

$$I(x,y)=\left(\frac{I_{\mathrm{raw}}(x,y)-\mathrm{DF}(x,y)}{\mathrm{FF}(x,y)-\mathrm{DF}(x,y)}\right)[\mathrm{FF}(x,y)-\mathrm{DF}(x,y)]_{\mathrm{mean}}. \tag{2}$$

This calibration, however requires a uniform FF calibration image.[17] To achieve uniformity, an optimum thickness of solid water buildup has to be found. The EPID was calibrated with thicknesses of solid water buildup of 5, 7.5, 10 cm and no buildup. The flatness of the flood-field image for each calibration was examined using profiles through the central axis in cross-plane and in-plane directions. The calibration field size was 40×30 cm^2 at isocenter with the detector at a source–detector distance (SDD) of 105 cm. The solid water was placed on the detector surface and the accelerator positioned vertically downward. The detector was leveled to remove any sag due to the solid water.

Immediately following each calibration, the solid water was removed, and an image was acquired of a 20×20 cm^2 open field. This open field image has the flood-field correction for the previous calibration applied. Thus four open field images were acquired, each with identical input fluence to the detector (no buildup on EPID), but with different flood-field corrections corresponding to 0, 5, 7.5, and 10 cm of solid water buildup. These open field images were then compared to ion-chamber measurement at $d_{\max}$, to see whether the EPID image, with flood-field correction corresponds to the ion chamber. The ion-chamber measurement was recorded in a water tank with a 0.125 cc ion chamber (Wellhofer Dosimetrie, Schwarzenbruck, Germany) at 1.5 cm depth at a source–surface distance (SSD) of 100.0 cm for the same field size.

C. Dosimetric properties

1. Effect of buildup

To determine whether added buildup material was required for accurate dosimetry, the effect of added buildup placed on the detector surface on the EPID response for the 6 MV beam was investigated. The 1 mm copper plate and scintillator screen provides inherent buildup. Solid water of thickness 0.5, 1.0, and 1.5 cm were placed on the collision

cover surface leaving a gap of ~2.5 cm to the amorphous silicon. Open field images of a 10×10 cm^2 field were acquired with the EPID at 105 cm from the source. Ten frames were averaged for each image. The images were acquired with a delay after the beam was turned on so that the accelerator dose rate had stabilized. The mean and standard deviation of the pixel values in a 10×10 pixel region at the center of the field were recorded for each solid water thickness.

Images of open fields of size 5×5, 10×10, and 20×20 cm^2 were then recorded as above with the EPID with and without the buildup material present. Profiles through the central axis were obtained. The beam profiles with and without the buildup material present were compared.

2. Dose response

As the EPID image is the average of acquired frames, two images acquired with different dose or monitor unit settings should result in the same pixel values provided the dose rate and hence dose/frame is the same. The pixel values will, however, be sensitive to dose rate as this will change the dose per frame. To obtain a measure of integrated dose from the images, the pixel values must therefore be multiplied by the number of frames acquired [Eq. (1)].

The linearity of the EPID to variations in dose rate was investigated by comparison to ion-chamber measurements. To modify the dose rate the SDD was varied by varying the distance below isocenter (5.5, 20.2, 30.2, 40.1, 53.1, 64.4, and 83.5 cm). No extra buildup was utilized on the EPID. At each distance, three images of a 5×5 cm^2 field were acquired and the mean pixel values in a 10×10 pixel region at the center of each field were recorded. Each image consisted of ten averaged frames acquired following a delay after the beam was turned on. This delay ensured stability of the accelerator dose rate. To determine the relative dose rate with distance, the 0.125 cc ion chamber was placed in a perspex mini-phantom at a 3 cm depth at each SDD.

To verify linear response with dose, images of a 10×10 cm^2 open field were acquired. The EPID was positioned at a fixed detector distance of 105.0 cm, and varying dose was delivered with monitor unit (MU) settings of 10, 20, 50, 100, and 200. For each MU setting, frames were continuously averaged during the irradiation. The pixel values at the center of the field were obtained as described earlier and were then multiplied by the number of frames acquired for each image. The linearity of delivered dose with MU setting was verified by ion-chamber measurement in the mini-phantom.

3. Field size response

The field size response of the EPID was compared to ion-chamber measurement. The detector was positioned at 105 cm from the source and field sizes defined by the multileaf collimators were varied from 4×4 to 24×24 cm^2. Three images were acquired for each setting with no added buildup on the EPID. The images were acquired with ten frames after dose-rate stabilization and pixel values recorded as described earlier. To record the change in dose with field size, ion-chamber measurements were performed at a depth of 1.5 cm in a solid water phantom with 5 cm of backscatter, and 105.0 cm to the chamber. Both sets of measurements were normalized to the 10×10 cm^2 values.

4. Effect of dead time in frame acquisition

The EPID system has a dead time in frame acquisition occurring every 64 frames. The ACPU is capable of adding up to 64 frames in its 20 bit hardware memory (frame-buffer). Every 64 frames the content of the frame-buffer is moved to the 32-bit-wide DRAM of the CPU. This transfer takes ~0.16 s. A reset frame (non-image frame) is then acquired.[15] This represents a dead time in image acquisition of ~0.28 s every 64 frames, approximately equivalent to a loss of two image frames. As radiation is continuously delivered during this dead time, the effect of the dead time on recording dynamic IMRT was investigated. Sliding window deliveries were performed with a uniform 1 cm leaf gap between the two banks of multileaf collimator (MLC) leaves and a 10×10 cm^2 field. Three leaf speeds of 0.25, 0.5, and 1.0 cm s^{-1} were created by modifying the MU setting. This pattern should result in a uniform beam profile and is utilized as a quality assurance test of leaf-speed stability.[18] Images were acquired by continuously averaging frames. Profiles were obtained along the direction of leaf motion directly under the center of the MLC leaf adjacent to the central axis. Reduction in signal from a uniform profile occurring due to the dead time in frame acquisition was quantified for each leaf speed.

5. Response with leaf speed

Leaf speeds of up to 2.5 cm s^{-1} are utilized at our center for DMLC delivery. If the EPID pixels integrate the dose between consecutive frame read-outs, then leaf speed or frame rate should not affect the acquired signal. However, if signal is collected for only a portion of the frame time, or if the pixels saturate before frame readout then errors in the signal may occur. It is important therefore to ensure that the EPID accurately records the rapid changes in dose rate to a pixel that occur during DMLC radiation delivery. Sliding window deliveries were performed with a uniform 1 cm leaf gap between the two banks of MLC leaves for a 10×10 cm^2 field. The leaf speed was varied from 0.33 to 2.5 cm s^{-1} by varying the number of monitor units. Three images were acquired for each leaf speed with continuous frame averaging, and the image values multiplied by the number of frames acquired. Profiles under the center of the MLC leaf adjacent to the central axis were analyzed to obtain the EPID signal for each leaf speed. These were compared to ion-chamber measurements made in the mini-phantom for each leaf speed at the center of the field under the center of the same MLC leaf.

6. Response to dose-rate fluctuations

The readout of the amorphous silicon array is synchronized with the beam pulses. The EPID is also calibrated at each fixed accelerator dose rate (e.g., 400 MU/min) used for

clinical imaging. The DF and FF images are different for each dose rate due to variation in the dose rate and image acquisition timing. During IMRT treatments if the MLC leaves cannot reach a pre-defined position with maximum leaf speed then beam hold-offs result where the accelerator reduces dose rate (''holds-off beam'') until the leaves have reached the desired position. This can result in large dose-rate fluctuations during the delivery. Potentially these could affect the EPID signal where the EPID system is designed and calibrated with a fixed accelerator dose rate. The effect of beam hold-offs on the EPID signal were examined by recording a ''step-wedge'' IMRT pattern with and without beam hold-offs. For the pattern, dose settings of 50 and 500 MU were utilized to deliver the field with and without beam hold-offs. During the 50 MU irradiation the beam dose rate fluctuated to less than 200 MU/min at times during the delivery. Beam profiles directly under the leaf adjacent to the central axis were obtained from the EPID images and compared.

7. Memory effect

The memory effect of the EPID was studied in a manner similar to that utilized by van Esch *et al.*[6] for the liquid ion-chamber EPID. An image was acquired with a 5×5 cm^2 field size, followed immediately by an image of a 20×20 cm^2 field size. The interval between the two images was approximately 15 s. A memory effect of the EPID will manifest as an increase in the pixel value for the 20×20 cm^2 field size in the region of irradiation of the 5×5 cm^2 field. An image was acquired of the 20×20 cm^2 field after several minutes had elapsed for comparison. Profiles across the 20×20 cm^2 field images were compared to see whether the pixel value was elevated due to a memory effect.

8. Relative dosimetry

The accuracy of the EPID in recording open and wedged static fields was investigated. Images were acquired with open fields from 5×5 up to 20×20 cm^2. These images were acquired with ten frames following dose-rate stabilization. The EPID was positioned at 105.0 cm from the source with no added buildup material. Similarly images were acquired with 45° and 60° steel wedges for field sizes of 20×20 and 15×15 cm^2, respectively. The transmitted beam contains some variation in beam energy across the field (in the wedged direction) due to the varying thickness of steel. EPID profiles through the central axis for the open fields and in the wedged direction for the wedged fields were compared to ion-chamber measurements recorded at 1.5 cm depth in a water phantom at 100.0 cm SSD. The EPID result was scaled to 101.5 cm to enable comparison, assuming there would be no change in EPID measurement at 101.5 and 105 cm distances apart from beam divergence.

IMRT test patterns were recorded with the EPID using continuous frame-averaging mode and compared to film measurement. A bar-pattern test fluence was created with an in-house software package. This fluence consisted of bar patterns of different spatial frequencies, with the highest frequency having 1 cm bars spaced at 2 cm intervals. This was input to the RTPS as an ''optimal fluence map'' and the RTPS then calculated leaf trajectories and a ''deliverable'' or ''actual'' fluence map. These were recorded on the 6 MV accelerator with Kodak XV film (Eastman-Kodak, Rochester, NY) at 1.5 cm depth in a solid water phantom. The films were digitized with a Vidar scanner (Vidar Corp, Herndon, PA) and converted to relative dose with a measured calibration curve.

For pre-treatment verification of the IMRT fluence delivery, the EPID image can either be compared to a predicted PDI, or converted to a ''fluence'' image for comparison to the expected fluence without the patient present. To investigate the potential of the EPID for this application, an image was acquired of a clinical IMRT field and compared to the fluence map utilized by the RTPS for the dose distribution. The field was from a clinical six field parotid plan. Profiles in the leaf motion direction were compared at the central axis and at off-axis planes.

9. Reproducibility

The reproducibility of the EPID signal is particularly important if the EPID is to be utilized to record not only relative dose measurements but also record absolute dose variations. The reproducibility was assessed by recording a step-wedge IMRT delivery on multiple occasions over a period of one month. This pattern consisted of five uniform intensity levels (bars) with relative intensities of 0.2, 0.4, 0.6, 0.8, and 1.0. At each measurement the EPID was set up at the same position. The differences between profiles through the central axis of the field were quantified and the standard deviation calculated.

III. RESULTS

A. EPID calibration

The effect of the thickness of solid water utilized when recording the FF calibration image is shown in Fig. 1(a). This shows profiles through the central axis of the FF images recorded with no buildup, 7.5 cm buildup, and 10.0 cm solid water buildup on the EPID. The FF profile with 10 cm buildup is relatively flat, while the profile with no buildup increases rapidly off-axis. Figure 1(b) shows EPID measurements (with no buildup on the EPID) of an open 20×20 cm^2 field. The EPID images have been divided by the FF calibration images from these three different buildup thicknesses. These EPID profiles, again obtained through the central axis in the cross-plane direction, are compared to ion-chamber measurement at 1.5 cm depth in a water tank. For clarity the 5 cm of solid water result, which was between the zero and 7.5 cm thickness, has been omitted.

The EPID calibrated with no buildup shows an underestimation of the beam profile as measured with the ion chamber. The FF image in this case reduces the pixel values off-axis. The result when the EPID was calibrated with between 5.0 and 7.5 cm of solid water closely matched the measured ion-chamber profile (within 2%). There was reduced agree-

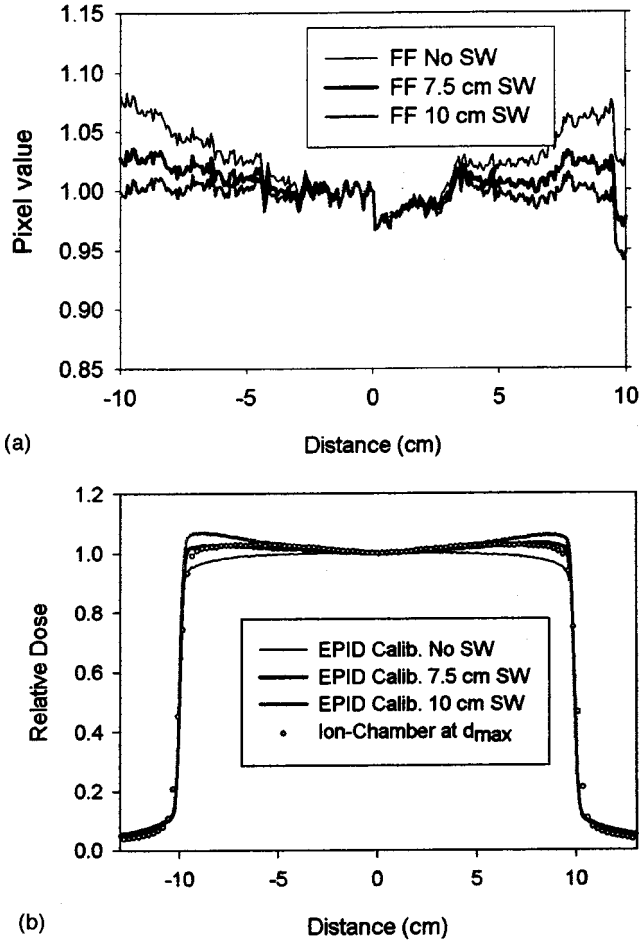

FIG. 1. (a) EPID flood-field (FF) calibration profiles, through the central axis, recorded with no buildup, 7.5 cm buildup, and 10.0 cm solid water buildup on the EPID. (b) EPID image profiles (with no buildup on the EPID) through the central axis of an open 20×20 cm^2 field. The EPID images have been divided by the FF calibration images taken with the three different buildup thicknesses. These open field profiles are compared to ion-chamber measurements at d_{max} depth in a water phantom.

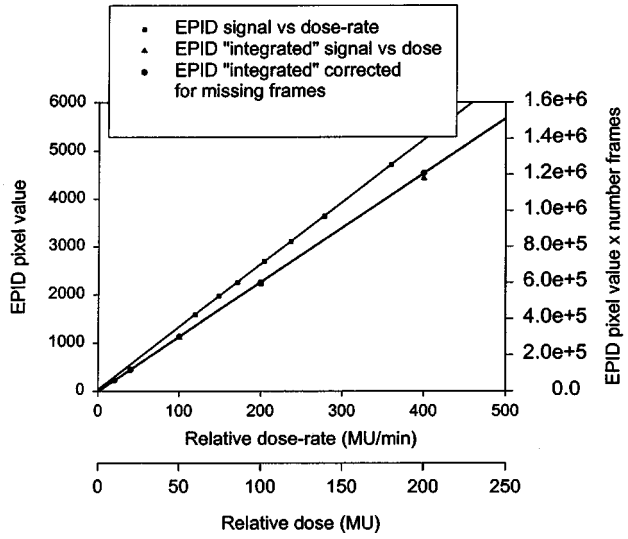

FIG. 2. Linearity of the EPID with dose rate and integrated dose. The dose rate to the EPID was varied by varying the source to detector distance. Ion-chamber readings were recorded at each EPID position in a mini-phantom to determine the relative dose rate. The relative dose rate is expressed in MU/min assuming a nominal output of 400 MU/min at 100 cm from the source. A measurement of integrated dose was obtained by multiplication of the image pixel values by the number of frames averaged, with and without correction for dead time in image acquisition. These were also compared to ion-chamber readings.

ment of EPID and ion chamber with addition of 10 cm of solid water. The EPID was calibrated with 6.0 cm of solid water for the following measurements.

The EPID profiles measured in the in-plane direction exhibited a gradient that closely matched (but in the opposite direction) a gradient observed in the FF measurement. This is consistent with the FF being the source of this gradient. The gradient was not symmetric about the EPID center, being approximately 0.2% per cm in the top half of the image and approximately 0.6% per cm in the bottom half of the image. Investigations were performed to identify the source of the gradient in the FF image. The angle of the EPID surface was leveled and the FF remeasured, however this did not remove the gradient. It was however observed that when EPID FF acquisition was initiated during calibration, the accelerator dose rate reduced from 400 to ~370 MU/min. It was our practice to wait for the accelerator dose rate to stabilize at 400 MU/min before initiating the FF acquisition. It is possible that this gradient is due to the reduction in dose rate occurring during the acquisition of frames of the FF, introducing a gradient through these frames and hence into the FF image, although this was not confirmed.

B. Dosimetric properties

1. Effect of buildup

For the 0, 0.5, 1.0, and 1.5 cm thicknesses of added buildup the mean EPID pixel values were 99.4%, 100.0%, 98.8%, and 94.7% of the maximum reading, which was obtained for 0.5 cm of added buildup. The results from three separate irradiations agreed to within 0.2% (1 standard deviation). The signal is a maximum for an additional 0.5 cm of solid water, and decreases for larger thicknesses. The EPID signal corresponding to no extra buildup is within 1% of the maximum (at 0.5 cm buildup) due to the inherent buildup provided by the copper plate and other detector components. The profiles for the open fields with and without the 0.5 cm of solid water buildup were also within 1%. The effect of the extra buildup was only evident in a slight blurring of the penumbra. Therefore no extra buildup was utilized in the following measurements. For dosimetric measurements without a patient or scattering material present there is no necessity indicated here for extra buildup at this energy.

2. Dose response

The linearity of the EPID with relative dose-rate as measured by the ion chamber is shown in Fig. 2. A linear fit has been applied to the measurements. The relative dose-rate axis is expressed in terms of nominal accelerator dose rate with a dose rate of 400 MU/min at 100.0 cm from the source.

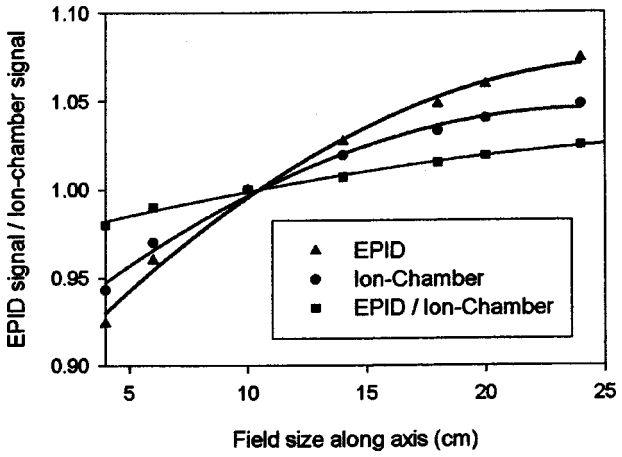

FIG. 3. Field size response of the EPID. The EPID signal change with field size is compared to the change in dose with field size measured with an ion chamber at 1.5 cm depth in a solid water phantom. The data are normalized to the 10×10 cm^2 field. Also shown is the ratio of the EPID readings to the ion-chamber readings.

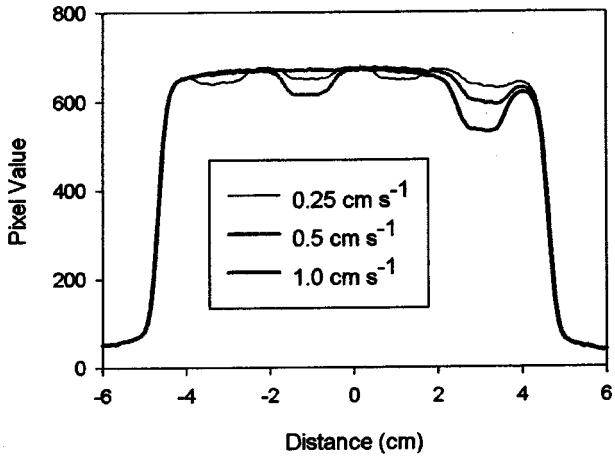

FIG. 4. The effect of the EPID dead time on recorded signal. A uniform sliding window delivery of 1 cm width was utilized over a 10 cm distance with leaf speeds of 0.25, 0.5, and 1.0 cm s^{-1}.

The three measurements at each distance differed by less than 0.2% (1 standard deviation) in all cases.

The linearity with integrated dose was investigated by delivering different monitor unit settings with the detector at a single distance and multiplying the resulting pixel values by the number of frames acquired. Due to the dead time in image frame acquisition, the number of frames for the increasing dose settings was not linear, with a reduction of two frames for each dead time occurring during the acquisition. For the MU settings of 10, 20, 50, 100, and 200, the number of frames acquired was 12, 24, 60, 118, and 234. Two frames are ''missing'' for the 100 MU (1 dead time) and 6 frames for the 200 MU (3 dead times), with the dead time occurring at 64 frame ($\sim$53 MU) intervals. For this static field delivery (constant dose rate) the pixel values accurately represent the dose rate to the detector as the ACPU is including only the actual acquired frames and therefore the frame-averaged reading [Eq. (1)] does not include dead-time frames. However the calculated integrated dose obtained by multiplication of the pixel values by the number of frames is then too low, as the number of frames does not represent the irradiation time (for $>$64 frames). Alternatively the pixel values could be multiplied by the total time for the irradiation, or a corrected number of frames. This will only produce accurate dosimetry for static fields where the dose rate is constant. The data in Fig. 2 show the frame-averaged pixel values multiplied by the number of frames, and also by the number of frames expected with no dead time (equivalent to multiplication by total irradiation or imaging time).

3. Field size response

The EPID and ion-chamber readings with field size normalized to the 10×10 cm^2 values are shown in Fig. 3. Also shown is the EPID signal divided by the ion-chamber measurements. The EPID pixel values for the three separate irradiations were within 0.1% (1 standard deviation). Second-order polynomials have been fitted to the data. The EPID shows a field size response (relative to 10×10 cm^2 field) compared to ion chamber of -2% for a 4×4 cm^2 field and $+2.5\%$ for a 24×24 cm^2 field when compared to readings in solid water.

4. Effect of dead time in frame acquisition

The effect on the beam profile of the dead time in frame acquisition is shown in Fig. 4. These profiles were taken from the images of the uniform sliding window irradiation of 1 cm leaf gap with leaf speeds of 0.25, 0.5, and 1.0 cm s^{-1}. The profiles were obtained under a central MLC leaf along the direction of leaf motion. The profiles should be uniform however reductions are evident with $\sim$1 cm width at intervals that correspond to 64 frame intervals in the image acquisition. The errors in this case are large even for the relatively low leaf speeds. The measured maximum errors as a function of the leaf speed are shown in Fig. 5. These values represent the reduction in EPID signal due to the dead time

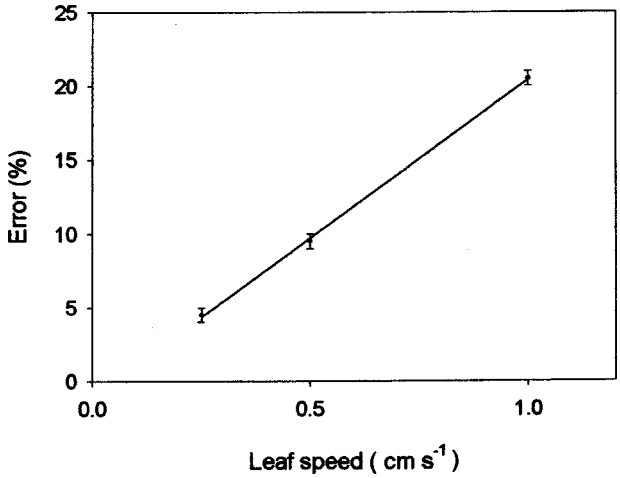

FIG. 5. Errors in EPID signal due to dead time as a function of the leaf speed for a 1 cm gap sliding window delivery with leaf speeds of 0.25, 0.5, and 1.0 cm s^{-1}.

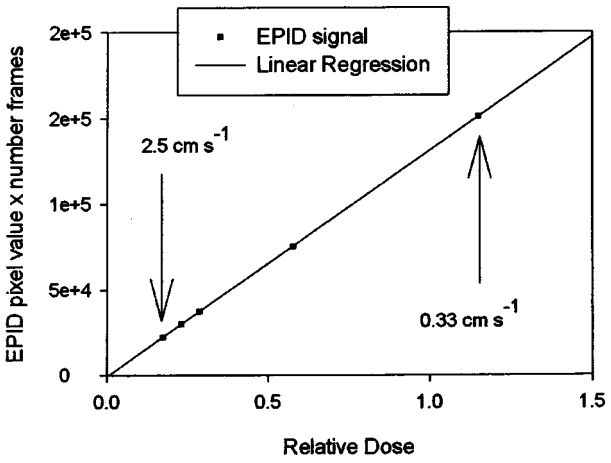

FIG. 6. Linearity of the EPID signal with leaf speed. The linearity was investigated up to 2.5 cm s^{-1} leaf speed. This demonstrates that the EPID can record the rapid temporal changes in dose rate that occur during DMLC deliveries. This analysis was performed in areas of the image only slightly affected by the dead time.

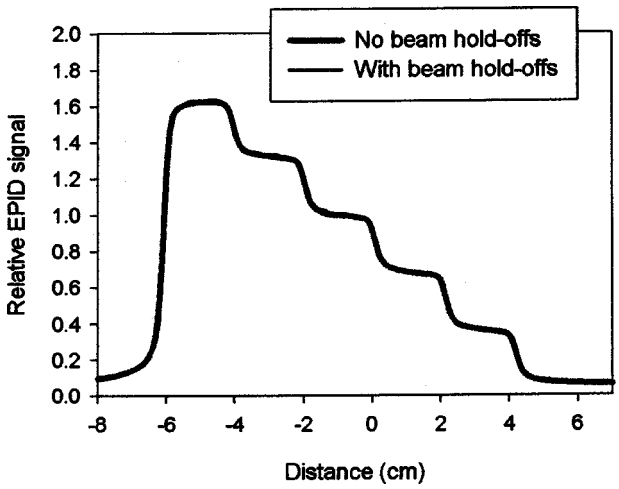

FIG. 7. Comparison of measured EPID profiles of an IMRT test pattern with and without beam hold-offs. The dose rate dropped from 400 MU/min to below 200 MU/min during the delivery of the pattern with 50 MU, while the 500 MU delivery maintained a consistent dose rate of ~370 MU/min.

expressed as a percentage. The maximum error increases linearly with leaf speed. The dead time results in large reductions in the EPID signal for faster leaf speed. This is due to the fact that when the leaves are moving rapidly, each portion of the detector is irradiated for only a short time. For example for a 1 cm leaf gap moving at 1.0 cm s^{-1}, each 1 cm width region on the detector (with the detector at 100 cm from the source) is only irradiated for 1 s. The 20% maximum error in signal for the 1.0 cm s^{-1} leaf speed due to the dead time observed here corresponds reasonably well with a dead time of ~0.28 s. Therefore even a small dead time can result in a large loss of signal. When less than 64 frames were utilized for image acquisition there was no nonuniformity of the profile observed. The large errors would manifest as errors in the lower signal areas of IMRT irradiations and for fields with small numbers of MU, however the errors are still significant even for slow leaf speed.

5. Response with leaf speed

Figure 6 illustrates the EPID signal linearity with leaf speed. The EPID pixel values have been multiplied by the number of frames to obtain an integrated pixel value. This shows that the EPID is accurately recording the rapid changes in dose rate. These results were obtained by analysis of profiles across sliding window deliveries, and compared to ion-chamber readings in a mini-phantom. These profiles exhibited reductions in signal in the region of the image under the open MLC leaf gap due to the dead time of the EPID every 64 frames as seen in Fig. 4. The values utilized for Fig. 6 were obtained from regions of the image that during the dead time were irradiated only by MLC transmission, and hence only slightly affected. Three images were recorded for each leaf speed and the pixel values obtained in each case were within 0.2%.

6. Response to dose-rate fluctuations

The agreement between the test pattern recorded with and without beam hold-offs is shown in Fig. 7. Slight fluctuations in signal are evident for the pattern recorded with beam hold-offs however these are not significant (less than 1%). The calibration and synchronization of the EPID at a fixed accelerator dose rate does not appear to limit the accuracy of the EPID when the accelerator dose rate varies from this.

7. Memory effect

The image of the 20×20 cm^2 open field acquired shortly after the 5×5 cm^2 field exhibited a faint "ghosting" of the 5×5 cm^2 field that was visible after extreme window/leveling to improve the contrast. However this ghosting was very small, at less than 0.2%. This result suggests that the memory effect is not significant in this time interval between image acquisition.

8. Relative dosimetry

The agreement between the EPID profiles and ion-chamber measurements was within 3% for the open and wedged fields inside the penumbral region. An example is shown in Fig. 8 for a 60° wedge with a 15×15 cm^2 field, where the EPID profile through the central axis in the wedged direction is compared to ion chamber. The data are normalized to the central axis point. These results suggest that the EPID should be a useful device for verification of static field delivery, and for quality assurance purposes such as beam profile constancy.

Figure 9 shows an example of agreement between EPID and film for the highest frequency IMRT bar pattern, with the data normalized to the central axis. The agreement is within 5%, with the main discrepancies occurring in the trough regions of the pattern. The level of agreement with the lower frequency bar patterns was similar, however the discrepancies in the trough regions were not apparent. To validate the

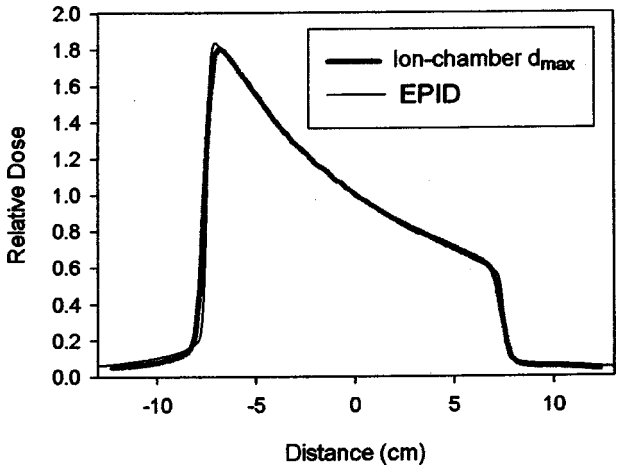

FIG. 8. Example of the EPID measurement of wedged static fields. The EPID measurement of a 60° physical wedge for a 15×15 cm^2 field compared to ion-chamber measurement at 1.5 cm depth in water.

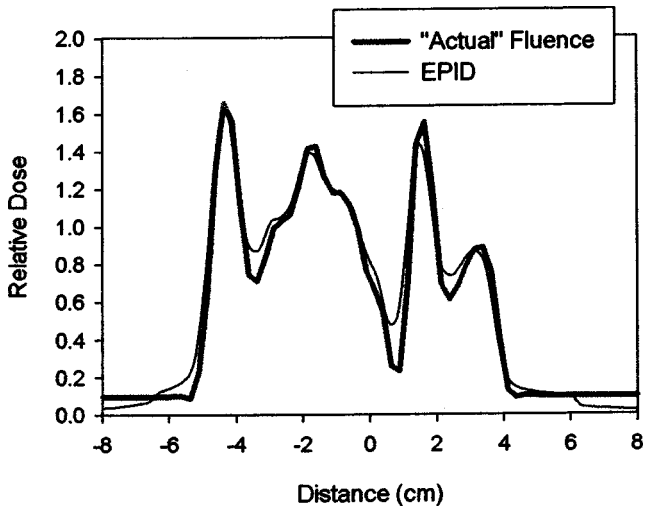

FIG. 10. Comparison of EPID image with the actual fluence map utilized by the RTPS system for dose-distribution calculation.

use of film for comparison to the EPID, film measurements of 10×10 and 20×20 cm^2 open field profiles at 1.5 cm depth in solid water were compared to ion-chamber measurements recorded in a water phantom. Agreement of the film and ion chamber for the open field profiles was within 2% in the high-dose region and within 3 mm in the penumbral region.

A comparison of an EPID profile for the clinical IMRT field and the actual fluence file utilized by the RTPS is shown in Fig. 10. The agreement is reasonable considering that the EPID is compared with the raw fluence map, with no explicit calculation of the PDI at the EPID plane. The effects of the accelerator source, MLC transmission, and EPID scatter have not been incorporated. The agreement was similar for other profiles through the irradiated field. The EPID obviously shows promise to verify the IMRT delivery by comparison to PDIs calculated from the RTPS fluence.

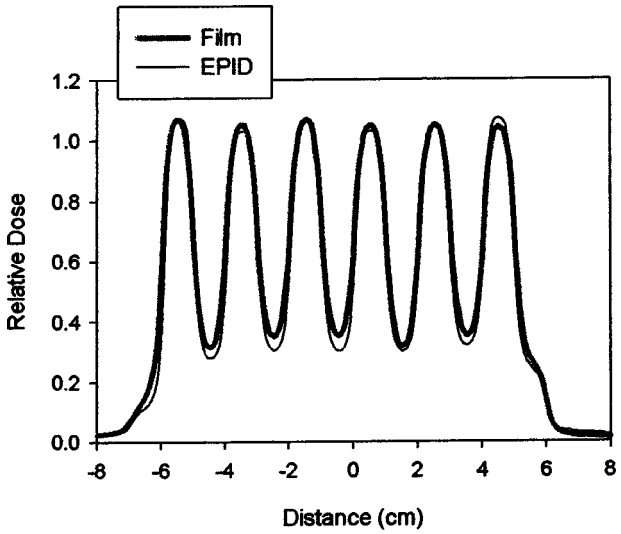

FIG. 9. Example of an EPID profile for the highest frequency bar-pattern IMRT field compared to a film measurement at 1.5 cm depth in solid water.

9. Reproducibility

The differences between the same IMRT delivery recorded at intervals over a period of a month was 0.8% (1 standard deviation) in the regions of relatively uniform irradiation. In regions of steep dose gradient, the result is affected by offsets of the different images due to slight differences in detector positioning. In these regions the separation of the intensity edges was within 0.5 mm. The EPID shows a high degree of reproducibility. Images of the same pattern were also taken pre- and post-flood-field calibration of the EPID and compared. These were within 0.2% (1 standard deviation). This was also repeated with a change in the calibration thickness of solid water from 6.0 to 7.5 cm. The pixel values then exhibited a uniform offset of ~1% due to the change in the FF correction with the increased thickness of solid water.

IV. DISCUSSION

The performance of the amorphous silicon detector was assessed for pre-treatment dosimetric measurement of IMRT beam delivery. The effect of a patient in the beam on the IMRT fluence and on measurement with this detector was not assessed. However the properties investigated here will also generally apply to the use of the EPID for *in vivo* dosimetry. Image acquisition for IMRT verification was performed by acquiring a single image comprised of multiple image frames. These frames are rapidly acquired at ~0.125 s and the resulting image is the average of all the image frames. This is necessary as the acquisition of multiple single images during the delivery has a delay of ~2 s between images. Large numbers of images would also be generated in this approach. Integration of the entire dose delivery from a single frame is not possible as the detector saturates at relatively low doses.

The calibration of the EPID with a FF image is important for accurate dose response as all acquired images are divided by the normalized FF image. This image is acquired to correct for non-uniformities in the EPID response, and ideally the input beam profile for the FF acquisition should be uniform. Although the FF image acquired with 10 cm of solid water was relatively flat, the open field measurement with this FF correction applied was higher than ion chamber. A potential explanation is that the EPID over-responds with increasing distance off-axis. This is apparent in the FF profile for no buildup on the EPID which is higher off-axis than the true beam ''horns.'' Therefore a FF correction image that contains an approximation to this over-response can result in better agreement with measurement than a flat FF image.

A gradient was also introduced into the calibration FF image, potentially due to the accelerator dose-rate reduction during the acquisition of this image. To overcome this a gradient correction can be applied to all acquired images, or potentially the gradient can be removed from the flood field if this effect is reproducible and stable. The influence of the calibration FF was also found to be important by Parsaei *et al.*[17] for the liquid ion-chamber EPID, where they utilized 10 cm of solid water to calibrate the EPID. Software tools for the user to verify the flatness of the calibration FF image for accurate dosimetry would be a useful addition to the calibration software module.

The change in dose with added buildup on the detector corresponds within 1.3% to percentage depth dose data assuming an inherent water-equivalent buildup of the EPID of 1.0 cm. This is reasonable assuming a copper plate density of 8960 kg/m^3, and the additional buildup from the 0.5-mm-thick scintillator (that includes a 0.18 mm polyester reflector). There was a small increase in EPID signal with additional buildup of 0.5 cm. However as this was less than 1% and as there was little change in profiles recorded with the EPID, additional buildup was not utilized in this investigation. Were the EPID to be utilized with the patient present then buildup may be required to remove contaminant electrons from the patient.[6] However for pre-treatment fluence verification, there is no requirement found here for added buildup on the detector. If higher energies are utilized then the requirement for buildup would have to be reassessed.

The linearity of the EPID to dose and dose rate is an important property of the amorphous silicon device as dose calibration conversion of acquired pixel values to relative dose is not required. Linear behavior was also observed for prototype amorphous silicon EPIDs[12,13] and for this EPID model by McCurdy *et al.*[14] The cause of the field size response observed in the present study is not clear. This could be due to the increase in scattered radiation with increasing field size. Since the scatter has a low energy component, its effect on the EPID's phosphor response is enhanced compared to ion chamber due to the presence of high atomic number components in the phosphor.

In static field delivery the dead time in image acquisition reduces slightly the number of frames. Accurate dosimetry can be performed by multiplication of the pixel values by the total irradiation time or the number of frames corrected for dead time. The dead time does not affect the relative dose profile of the image for constant dose-rate irradiation as it affects all parts of the image equally.

This is not the case for DMLC delivery where only a portion of the detector is irradiated at a particular time. The dead time in frame acquisition occurring every 64 frames is identified as a major limitation of this device for DMLC fields. With the rapid leaf speeds during IMRT delivery, delays in sampling of the intensity have significant consequences. The errors observed here were over 20% for a leaf speed of 1.0 cm s^{-1} with a 1 cm gap between the leaves. The errors increased linearly with increasing leaf speed. As the leaf speed increases the time that a detector region is exposed to the beam is reduced and so a small dead time in sampling becomes more important. The error will also increase with decreasing leaf gap for the same leaf speed.

To overcome this problem the EPID images can be acquired with less than 64 frames. This however corresponds to only 8 s for beam delivery. Alternatively if a large MU setting is utilized then leaf speeds will be slower and the errors are kept small. A similar method was utilized by Chang *et al.*[16] for the liquid ion-chamber device to overcome the slow image acquisition speed. The correction of this dead time is difficult. The location of the major signal loss depends upon the locations and leaf speeds of each leaf pair during the dead time. Obviously this is a problem that the manufacturer will ultimately have to address.

The measurements performed for EPID response (accounting for the dead time) showed that the EPID can accurately record the rapid dose-rate changes that occur with leaf speeds of up to 2.5 cm/s. The EPID also accurately reflects the effect of beam hold-offs during the delivery. This means that the synchronization of the image acquisition with beam pulses is not crucial to accurate dosimetry. This was shown in Fig. 7 where an IMRT profile was recorded with and without dose-rate fluctuations. The memory effect was also investigated and was negligible over a time interval of $\sim$15 s. It is possible that the memory effect is greater for shorter time intervals. Investigation of the time decay of this memory effect would therefore be of interest. This was studied for the liquid ion-chamber EPID by acquiring multiple images after the irradiation had finished.[6] It was not possible with our detector system to acquire images after the beam had switched off, and the delay in each image would also be $\sim$2 s.

The comparison of EPID and ion-chamber results for static fields show that this device is applicable to dosimetry of static fields. The agreement of open and wedged fields was within 3%. There was no energy response apparent for wedged fields across the wedged direction. The variation in energy in this circumstance however is relatively small. Half-value layers for 3×3 cm^2 open field and 60° wedge fields at 6 MV calculated from percentage depth dose data are 11.5 and 12.5 cm, respectively. Previous work for metal/phosphor[19] and amorphous silicon systems[14] has shown that the energy response increases for lower energies such as scattered from the beam-defining system or the patient. This is potentially the reason for the higher EPID re-

sponse compared with ion chamber in the tails of the beam evident in Figs. 1 and 8. The potential utility of the EPID for quality assurance of beam flatness, symmetry, wedge angle is apparent. However a deficiency of the current system is that images cannot be acquired during enhanced dynamic wedge deliveries.

The agreement of EPID and film was found to be within 5% for IMRT fields. This agreement is promising considering the EPID signal in this study is essentially the raw response of the system. The only corrections applied to the data were the inherent FF and DF corrections. Further work is required to improve this for quantitative verification of IMRT. Film is currently widely utilized for IMRT verification due to its two-dimensional format and high spatial resolution.

The EPID signal was found to be very reproducible over a period of one month. This suggests that the EPID could be utilized for absolute dose verification. This is currently hampered by the EPID recording average dose per frame and not overall dose. To obtain a measure of dose, the image values must be externally multiplied by the number of frames (corrected for detector dead time) that were averaged, or alternatively the total irradiation time. The possibility of performing DMLC quality assurance is also enhanced by this finding, and this is currently being investigated at our clinic. Care should be taken when recalibrating the EPID, ensuring identical calibration conditions, to avoid a change in the FF correction. Alternatively, we are currently investigating whether the EPID can be utilized without regular recalibration.

The purpose of this work was to examine the fundamental performance of the amorphous silicon EPID as a detector for DMLC delivery of intensity modulated fields. The next stage of this project will be to utilize this understanding to facilitate accurate dosimetric measurements. These can then be compared to predicted PDIs for pre-treatment dosimetric verification of IMRT. The comparison of the measured EPID image and the actual fluence utilised by the RTPS shown in Fig. 10 demonstrate the potential of this device for IMRT delivered fluence verification.

V. CONCLUSIONS

Several properties of an amorphous silicon EPID for dosimetry of IMRT fields were assessed. The EPID has linear dose response and the signal is highly reproducible for IMRT verification. Sampling rate is adequate for the rapid MLC leaf speeds utilized during IMRT delivery. Calibration of the EPID with a uniform input beam profile (for nonuniform sensitivity) is required for accurate dosimetry. Limitations of the EPID system were identified including a field size dependent response, and errors due to a dead time in image frame acquisition. The amorphous silicon EPID shows promise as an efficient verification tool for IMRT delivery, the main limitation at present being the dead time in frame acquisition.

ACKNOWLEDGMENTS

The authors would like to acknowledge Julie Roberts, and Shawn Stapleton who developed the IMRT bar patterns and software to produce optimal fluence maps.

[a]Present address: Newcastle Mater Hospital, Locked Bag 7, Hunter Region Mail Center, NSW 2310, Australia; electronic mail: peter.greer@mater.health.nsw.gov.au

[1] B. Rhein and P. Häring, ''The IMRT phantom verification procedure at Heidelberg,'' Radiother. Oncol. **61**, S2 (2001) (abstract).
[2] C. Burman, C. Chui, G. Kutcher, S. Leibel, M. Zelefsky, T. LoSasso, S. Spirou, Q. Wu, J. Yang, J. Stein, R. Mohan, Z. Fuks, and C. C. Ling, ''Planning, delivery, and quality assurance of intensity-modulated radiotherapy using dynamic multileaf collimator: A strategy for large-scale implementation for the treatment of carcinoma of the prostate,'' Int. J. Radiat. Oncol., Biol., Phys. **39**, 863–873 (1997).
[3] X. Wang, S. Spirou, T. LoSasso, J. Stein, C. S. Chui, and R. Mohan, ''Dosimetric verification of intensity modulated fields,'' Med. Phys. **23**, 317–327 (1996).
[4] M. Essers, M. de Langen, M. L. P. Dirkx, and B. J. M. Heijmen, ''Commissioning of a commercially available system for intensity modulated radiotherapy dose delivery with dynamic multileaf collimation,'' Radiother. Oncol. **60**, 215–224 (2001).
[5] K. L. Pasma, M. L. P. Dirkx, M. Kroonwijk, A. G. Visser, and B. J. M. Heijmen, ''Dosimetric verification of intensity modulated beams produced with dynamic multileaf collimation using an electronic portal imaging device,'' Med. Phys. **26**, 2373–2378 (1999).
[6] A. van Esch, B. Vanstraelen, J. Verstraete, G. Kutcher, and D. Huyskens, ''Pretreatment dosimetric verification by means of a liquid-filled electronic portal imaging device during dynamic delivery of intensity modulated treatment fields,'' Radiother. Oncol. **60**, 181–190 (2001).
[7] K. L. Pasma, B. J. M. Heijmen, M. Kroonwijk, and A. G. Visser, ''Portal dose image prediction for dosimetric treatment verification in radiotherapy: An algorithm for open beams,'' Med. Phys. **25**, 830–840 (1998).
[8] K. L. Pasma, M. Kroonwijk, J. C. J. de Boer, A. G. Visser, and B. J. M. Heijmen, ''Accurate portal dose measurement with a fluoroscopic electronic portal imaging device (EPID) for open and wedged beams and dynamic multileaf collimation,'' Phys. Med. Biol. **43**, 2047–2060 (1998).
[9] F. F. Yin, M. C. Schell, and P. Rubin, ''Input/output characteristics of a matrix ion-chamber electronic portal imaging system,'' Med. Phys. **21**, 1447–1454 (1994).
[10] Y. Zhu, X.-Q. Jiang, and J. van Dyk, ''Portal dosimetry using a liquid ion chamber matrix: Dose response studies,'' Med. Phys. **22**, 1101–1106 (1995).
[11] M. Essers, B. R. Hoogervorst, M. van Herk, H. Landson, and B. J. Mijnheer, ''Dosimetric characteristics of a liquid-filled electronic portal imaging device,'' Int. J. Radiat. Oncol., Biol., Phys. **33**, 1265–1272 (1995).
[12] P. Munro and D. C. Bouius, ''X-ray quantum limited portal imaging using amorphous silicon flat-panel arrays,'' Med. Phys. **25**, 689–702 (1998).
[13] Y. El-Mohri, L. E. Antonuk, J. Yorkston, K. W. Jee, M. Maolinbay, K. L. Lam, and J. H. Siewerdsen, ''Relative dosimetry using active matrix flat-panel imager (AMFPI) technology,'' Med. Phys. **26**, 1530–1541 (1999).
[14] B. M. C. McCurdy, K. B. Luchka, and S. Pistorius, ''Dosimetric investigation and portal dose image prediction using an amorphous silicon electronic portal imaging device,'' Med. Phys. **28**, 911–924 (2001).
[15] Heinrich Riem, Varian Medical Systems, Baden, Switzerland, February, 2002 (private communication).
[16] J. Chang, G. S. Mageras, C. S. Chui, C. C. Ling, and W. Lutz, ''Relative profile and dose verification of intensity modulated radiation therapy,'' Int. J. Radiat. Oncol., Biol., Phys. **47**, 231–240 (2000).
[17] H. Parsaei, E. El-Khatib, and R. Rajapakshe, ''The use of an electronic portal imaging system to measure portal dose and portal dose profiles,'' Med. Phys. **25**, 1903–1909 (1998).
[18] C.-S. Chui, S. Spirou, and T. LoSasso, ''Testing of dynamic multileaf collimation,'' Med. Phys. **23**, 635–641 (1996).
[19] D. A. Jaffray, J. J. Battista, A. Fenster, and P. Munro, ''X-ray scatter in megavoltage transmission radiography: Physical characteristics and influence on image quality,'' Med. Phys. **21**, 45–60 (1994).